Selective Trans-Membrane Transport of Alkali and Alkaline Earth Cations through Graphene Oxide Membranes Based on Cation−π Interactions

Pengzhan Sun,[†] Feng Zheng,[†] Miao Zhu,[†,‡] Zhigong Song,[‡,§] Kunlin Wang,[†] Minlin Zhong,[†] Dehai Wu,[⊥] Reginald B. Little,[∥] Zhiping Xu,[‡,§] and Hongwei Zhu[†,‡,*]

[†]School of Materials Science and Engineering, State Key Laboratory of New Ceramics and Fine Processing, Key Laboratory of Materials Processing Technology of MOE, [‡]Center for Nano and Micro Mechanics, [§]Department of Engineering Mechanics, and [⊥]Department of Mechanical Engineering, Tsinghua University, Beijing 100084, P. R. China, and [∥]Department of Biological and Physical Sciences, South Carolina State University, Orangeburg, South Carolina 29117, United States

ABSTRACT Graphene and graphene oxide (G−O) have been demonstrated to be excellent filters for various gases and liquids, showing potential applications in areas such as molecular sieving and water desalination. In this paper, the selective trans-membrane transport properties of alkali and alkaline earth cations through a membrane composed of stacked and overlapped G−O sheets ("G−O membrane") are investigated. The thermodynamics of the ion transport process reveal that the competition between the generated thermal motions and the interactions of cations with the G−O sheets results in the different penetration behaviors to temperature variations for the considered cations (K^+, Mg^{2+}, Ca^{2+}, and Ba^{2+}). The interactions between the studied metal atoms and graphene are quantified by first-principles calculations based on the plane-wave-basis-set density functional theory (DFT) approach. The mechanism of the selective ion trans-membrane transportation is discussed further and found to be consistent with the concept of cation−π interactions involved in biological systems. The balance between cation−π interactions of the cations considered with the sp^2 clusters of G−O membranes and the desolvation effect of the ions is responsible for the selectivity of G−O membranes toward the penetration of different ions. These results help us better understand the ion transport process through G−O membranes, from which the possibility of modeling the ion transport behavior of cellular membrane using G−O can be discussed further. The selectivity toward different ions also makes G−O membrane a promising candidate in areas of membrane separations.

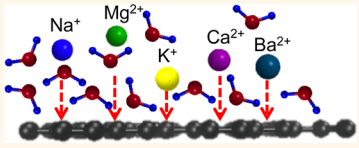

KEYWORDS: selective permeation · cation−π interaction · graphene oxide · alkali and alkaline earth cations · thermodynamics · first-principles calculations

The use of membranes composed of stacked and overlapped graphene oxide sheets (we call "G−O membranes") or nanoporous graphene films as filters for gases or liquid solutions has been reported.[1−6] For example, water molecules move through G−O membranes rapidly, but certain gases (He, H_2, N_2, and Ar) and liquids (ethanol, acetone, hexane, decane, and propanol) do not.[1] The anomalous perfect water permeation through the stacking G−O layers is attributed to the formation of hexagonal ice bilayer[2] between the flakes and the melting transition of ice at the sheet edges according to a recent simulation result (Scheme 1). The differing transport of ions dissolved in water can be achieved by G−O membranes with the faster transport of Na^+ relative to Mn^{2+}, Cd^{2+}, and Cu^{2+} and faster transport of certain strong acids (H_2SO_4) and bases (NaOH) compared to weaker acids and bases.[3] The nanoporous graphene membranes can be used as molecular sieves,[4] and a recent simulation result indicates that single-layer nanoporous graphene can effectively filter NaCl from water.[5] In addition, during the electrophoretically driven translocation of DNA through the nanopores within the graphene membranes, ultrahigh sensitivity to extremely small diameter changes of the translocating molecules can be achieved.[6] The above results all demonstrate the promising applications of G−O membranes and nanoporous graphene films in areas of separations.

In view of the structure of a single-layer G−O sheet, several types of oxygen-containing functional groups are present on the basal plane and the edges, resulting in small sp^2 regions isolated within the sp^3 matrix.[7] In terms of the ion-transport through G−O

* Address correspondence to hongweizhu@tsinghua.edu.cn.

Received for review October 25, 2013 and accepted January 8, 2014.

Published online January 08, 2014
10.1021/nn4055682

Scheme 1. Schematic Diagrams of the Ion-Transport Process and the Diverse Interactions between Different Cations and G−O Sheets[a]

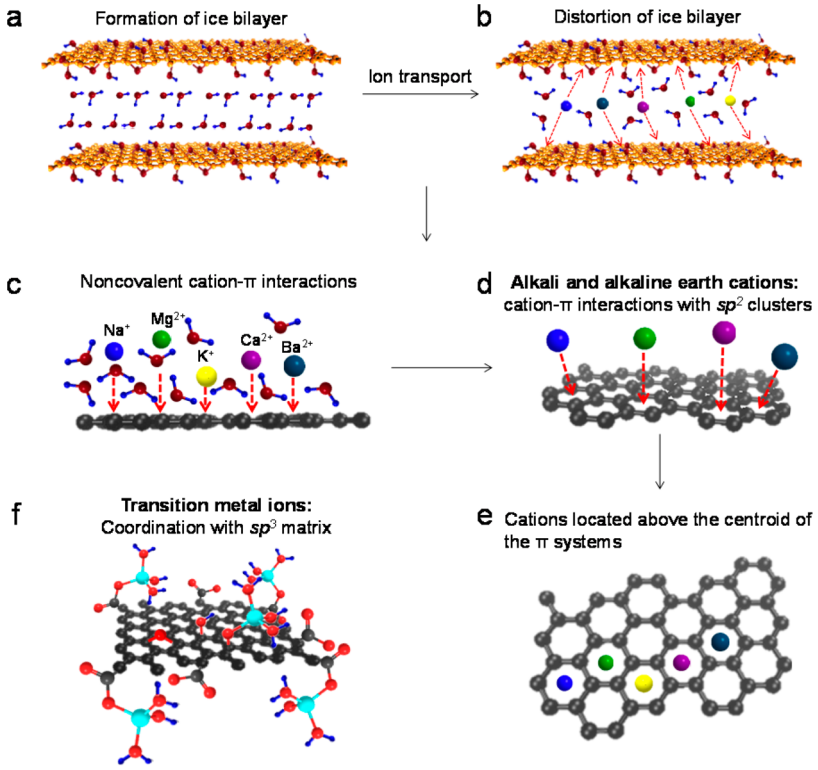

[a] Key: (a) formation of ice bilayer within the interlayer spacing of G−O flakes; (b) distorted structure of ice bilayer due to the interactions between cations and water molecules during the ion transport process; (c,d,e) noncovalent cation−π interactions of alkali and alkaline earth cations with the sp^2-clusters of G−O sheets; (f) coordination of transition metal ions with the sp^3 matrix of G−O sheets.

membranes, the coordination between transition metal ions and the functional groups decorated on G−O sheets is believed to be responsible for the ion-selectivity of G−O membranes (Scheme 1).[3] However, due to the presence of abundant sp^2 clusters, the cation−π interactions between the cations and the π systems may play a major role for the ion-recognition of G−O membranes toward cations with no *d* electrons, similar to some important ion transport process across cellular membranes.[8−10] The well-known cation−π interaction is a noncovalent interplay which describes the interaction between ions and the aromatic π-electron cloud. It plays a dominant role in some biological processes such as side-chain interactions in proteins, protein−ligand interactions, and ion channels and has been successfully utilized to interpret some important molecular recognition processes in biological systems.[8−10] It has been demonstrated to be of outstanding importance in determining the structure and function of supramolecular assemblies in materials science, catalysis, and chemical biology.[9,10] As alkali and alkaline earth cations are ubiquitous in biological systems, the understanding of the trans-membrane transport properties of these ions through G−O membranes is important, from which the modeling of the ion transport behavior of cellular membranes using G−O may be achieved further. In addition, the selective ion transport properties may endow the G−O membranes with potential applications in ion separations.

In this paper, we report on the study of transport into and through G−O membranes of alkali and alkaline earth cations (Na^+, K^+, Mg^{2+}, Ca^{2+}, and Ba^{2+}) with counter Cl^- anions. In addition to studies conducted at room temperature, the transport of these cations is also observed as a function of temperature from 10 to 40 °C, which helps us understand the thermodynamics of the ion penetration process through G−O membranes. To quantify the interactions between metal atoms and graphene, we perform first-principles calculations based on the plane-wave-basis-set density functional theory (DFT) approach. Finally, the mechanism for the trans-membrane transport behaviors of these cations through G−O membranes is discussed based on the cation−π interactions, which have been successfully utilized to interpret some important molecular recognition processes in biological systems.[8−10]

In our previous work on selective ion penetration through G−O membranes,[3] we speculated that the nanocapillaries formed within the G−O membranes might be responsible for the permeation of metal

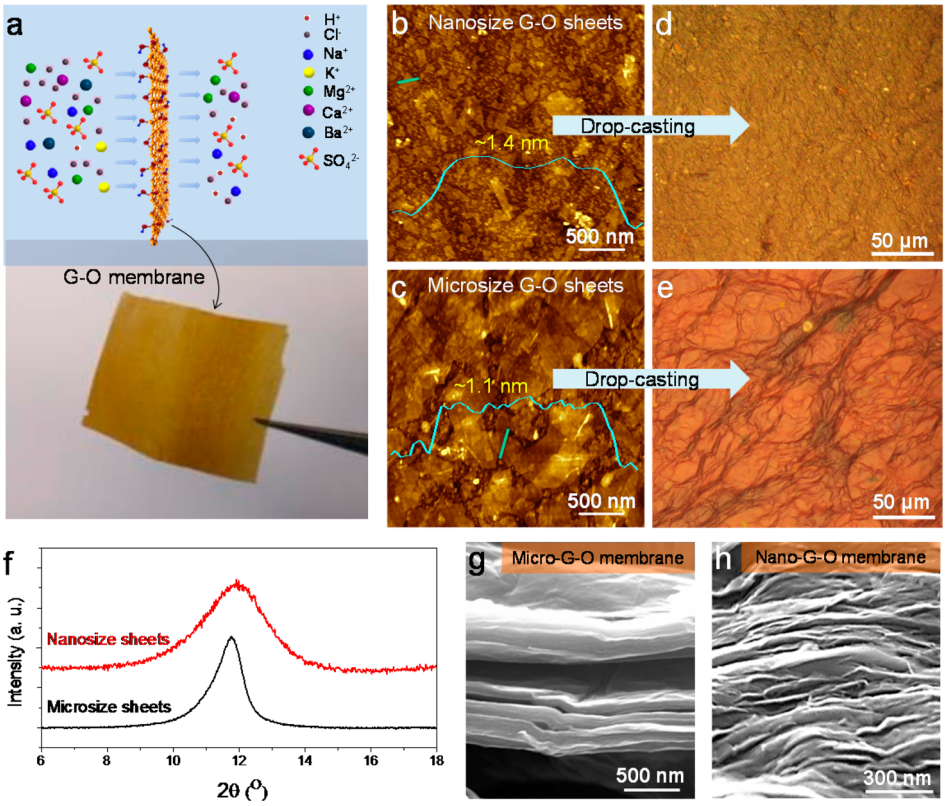

Figure 1. Schematics and characterizations of G−O membranes assembled by nano- and microsize G−O sheets. (a) Schematic diagrams of the penetration processes. (b,c) AFM images of as-prepared G−O sheets. (d,e) Optical images of drop-casted G−O membranes. (f) XRD spectra and (g,h) cross-section SEM images of G−O membranes prepared from microsize and nanosize G−O sheets, respectively.

cations and the strong coordination between transition-metal ions, and the oxygen-containing functional groups might give rise to the much slower permeation of heavy metal ions through G−O membranes compared to sodium salts. In this work, by comparing the ion penetration properties of G−O membranes prepared from nanosize and microsize sheets, respectively, we demonstrate experimentally that the nanocapillary networks formed within the lamellar membranes are indeed responsible for the ion trans-membrane transportation. Meanwhile, we extend the selectivity of G−O membranes to alkali and alkaline earth cations, in which *d* or *f* electrons are absent and the typical coordination interactions are not present. We demonstrate that the well-known cation−π interaction which is involved in some important molecular recognition processes in biological systems can also be employed in the ion-selectivity of G−O membranes, from which the application of G−O in fabricating artificial cellular membranes can be further discussed. The thermodynamics of the ion transportation through G−O membranes is studied which helps us better understand the interactions involved in the trans-membrane transport process of main group cations. Furthermore, first-principles calculations are performed and the results confirm our speculation that the cations lacking *d* electrons tend to interact with the sp^2 clusters through cation−π interactions while the transition metal ions mainly coordinate to the sp^3 matrix of G−O sheets.

RESULTS AND DISCUSSION

Characterizations of G−O Membranes. Figure 1a shows the schematic diagrams of the trans-membrane transport. When a drop containing a dispersion of G−O sheets was drop-casted onto a smooth paper and allowed to dry spontaneously, a piece of freestanding G−O membrane could be obtained (as shown in the inset of Figure 1a). Parts b and c of Figure 1 show atomic force microscopy (AFM) measurements of nanosize and microsize G−O sheets used in the experiments. The insets in parts b and c of Figure 1 show that the as-prepared G−O sheets are single-layered. Parts d and e of Figure 1 show optical images of G−O membranes comprised of either nanosize or microsize G−O sheets. These two types of G−O membranes possess different topographies: nanosize G−O sheets stack and overlap to form membranes with few wrinkles on the surfaces (Figure 1d), while the membranes formed from microsize sheets are "corrugated" with a large number of "wrinkles" (Figure 1e). The XRD diffractograms of the G−O membranes (obtained at the same relative humidity) prepared from nanosize versus microsize G−O sheets (Figure 1f) indicate that these two kinds of G−O membranes possess nearly the same

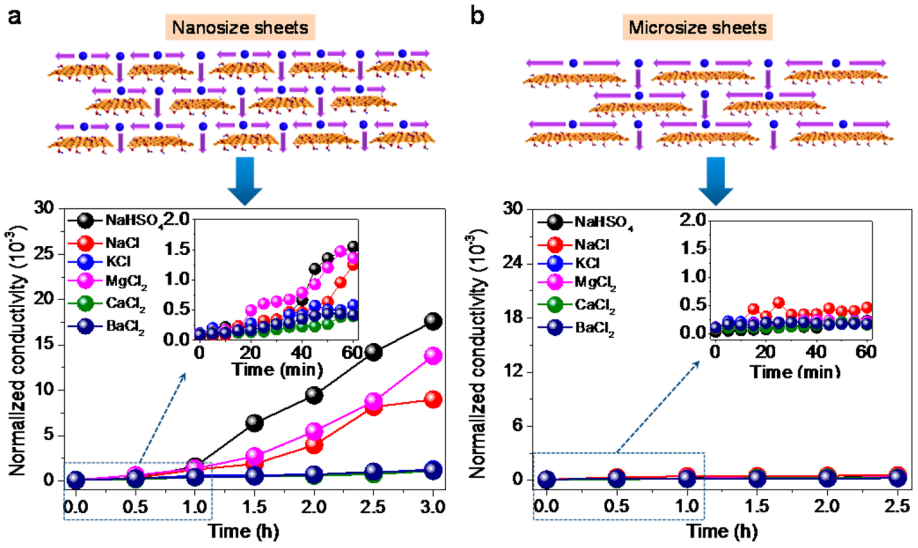

Figure 2. Schematics of the lamellar structures (top panels) and normalized conductivities of the filtrates of studied cations (bottom panels) for G–O membranes composed of (a) nanosize and (b) microsize G–O sheets. Insets show the initial stages (0–60 min) of the penetrations.

average interlayer spacing (~0.74 nm at a relative humidity of 30%). The cross-section SEM images in parts g and h of Figure 1 reveal the lamellar nature of the two different G–O membranes. The trans-membrane transport properties of alkali (Na^+ and K^+) and alkaline-earth cations (Mg^{2+}, Ca^{2+}, and Ba^{2+}) in water were investigated for these two types of G–O membranes prepared from G–O solutions with the same concentrations (3 mg/mL).

Penetration Tests. *Trans-Membrane Transport of Salt Ions through Nano-G–O Membranes.* The ion trans-membrane transport experiments were conducted with a homemade permeability apparatus (see the Materials and Methods and Figure S1). A 100 mL portion of certain aqueous solution (0.1 mol/L) and deionized water was injected with the same speed into the source and drain separated by G–O membrane. The conductivity variations of the drains were measured and plotted, which reflected the permeability of the ions investigated. Because the conductivity of a certain aqueous solution is relevant to the intrinsic nature (mass, size and charge, etc.) of the ions and in dilute solutions the conductivity is approximately proportional to the ion concentration, normalized conductivities of the drains were calculated (by dividing by the conductivity of the 0.1 mol/L source solutions), and these are plotted in Figure 2a. For G–O membranes prepared from nanosize G–O sheets (nano-G–O membranes) and at 20 °C, the relative transport rates of the cations were found to be $H^+ > Mg^{2+} > Na^+ > Ba^{2+}$, Ca^{2+} and K^+. The initial stages of ion transport into and through the G–O membranes are shown in the inset of Figure 2a. With normalization of the conductivities of the filtrates, all the penetrations increase slightly in a small level, indicating the retarded ion penetration in the initial stage, which is due to a gradual wetting process of the G–O membranes.

Trans-Membrane Transport of Salt Ions through Micro-G–O Membranes. For G–O membranes comprised of stacked and overlapped microsize sheets (micro-G–O membranes), the permeability of all the cations decreases significantly, as shown in Figure 2b, compared to nano-G–O membranes. When normalized conductivities are considered, it is seen that all the trans-membrane permeations increase just slightly during the whole process, demonstrating the significant resistance by micro-G–O membranes to the trans-membrane transport of these cations. When the dimension of G–O sheets within the membrane is changed from nanosize to microsize, the amount of the number of nanocapillaries formed within the G–O membrane is reduced significantly, resulting in the decrease of ion trans-membrane transportation in the case of micro-G–O membranes, as illustrated in the top panels of Figure 2a,b. (The conductivity variations of the drains for ion permeating nano- and micro-G–O membranes are shown in Figure S2, Supporting Information.) Unless otherwise specified, the subsequent ion trans-membrane transport experiments were all conducted with nano-G–O membranes due to the much faster ion permeation rates through the membranes prepared from nanosize G–O sheets.

Temperature-Dependent Penetrations. The thermodynamics of ion transport through G–O membranes was investigated. As shown in Figure 3, when the temperature is increased from 10 to 40 °C, the normalized conductivities of all the filtrates increase significantly during the whole process, indicating that the temperature increment promotes the ion-penetration through G–O membranes. In particular, for K^+ ions (Figure 3a), when the temperature is increased from 10 to 20 °C, the trans-membrane transport is not enhanced obviously. However, as the temperature is

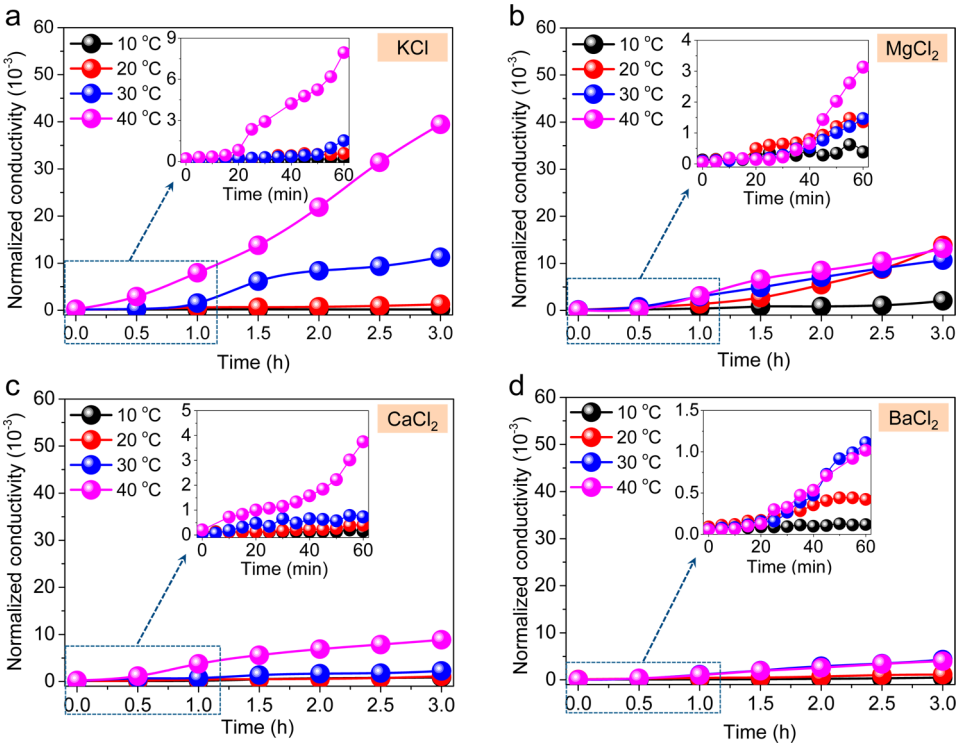

Figure 3. Temperature-dependent penetrations of alkali and alkaline-earth metal cations (10−40 °C): (a) KCl, (b) $MgCl_2$, (c) $CaCl_2$, (d) $BaCl_2$. Insets show the initial stages (0−60 min) of the penetrations.

increased further (from 20 to 40 °C), the penetrations are increased significantly and the increment for K^+ ions with temperature is much greater than for Mg^{2+}, Ca^{2+}, and Ba^{2+} ions. In the case of Mg^{2+} (Figure 3b), the increment of penetration with temperature from 10 to 20 °C is greater than those from 20 to 40 °C. As for Ca^{2+} (Figure 3c), only when the temperature is increased from 30 to 40 °C does the ion penetration have an obvious increment. In the case of Ba^{2+} (Figure 3d), there is a slight increase in penetration when the temperature is increased from 20 to 30 °C, while the trans-membrane transport changes little when the temperature is below 20 °C or above 30 °C. The detailed ion penetrations at initial stages are shown in the insets of Figure 3, revealing that the initial ion permeating abilities increase significantly with temperature. (The conductivity variations of the drains for ion transportation through nano-G−O membranes under different temperatures are shown in Figure S3, Supporting Information.)

In the ion-transport processes through G−O membranes, the normalized conductivity (penetration) can be expressed as the following Arrhenius equation: $\sigma/\sigma_0 = A \exp(-\varepsilon/kT)$, where σ/σ_0 is the normalized conductivity, A is the Arrhenius factor, ε is the activation energy, k is the Boltzmann constant, and T is the temperature. The activation energy of the ion transport process can be determined from the slope of the Arrhenius curve drawn from $\ln \sigma/\sigma_0 = \ln A - \varepsilon/kT$, as shown in Figure S4 (Supporting Information). It reveals that in the case of K^+ ions, the activation energy (determined from the slope of the Arrhenius curves) increases gradually with the penetration process, while the activation energies of Mg^{2+}, Ca^{2+}, and Ba^{2+} remain nearly unchanged during the whole transport process (Figure S4, Supporting Information). Notably, an inflection point exists in the Arrhenius curves of Mg^{2+}, Ca^{2+} and Ba^{2+} ions, indicating the presence of a sudden change of activation energy with temperature during the transport of alkaline earth cations (Figure S4b−d, Supporting Information). The above results demonstrate that the transport processes of considered alkali and alkaline earth cations into and through G−O membranes possess different thermodynamic behaviors, which may be due to the different interactions between the cations and G−O sheets (discussed later).

Ion Distributions within G−O Membranes. After ion penetrations, the G−O membranes were collected for Auger electron spectroscopy (AES) characterizations to determine the ion distributions within G−O membranes. As shown in Figure 4, it is seen that after the penetration of KCl, $MgCl_2$, $CaCl_2$, and $BaCl_2$ sources, there are nearly no Cl^- ions remaining within the G−O membranes, which is due to the negatively charged nature of G−O membranes in aqueous environment and the repulsive forces between Cl^- and the G−O sheets, while the cation distributions in G−O membranes are observed to differ significantly. After the penetration of K^+, the amount of K^+ remained within G−O membrane is small and distributes randomly along the

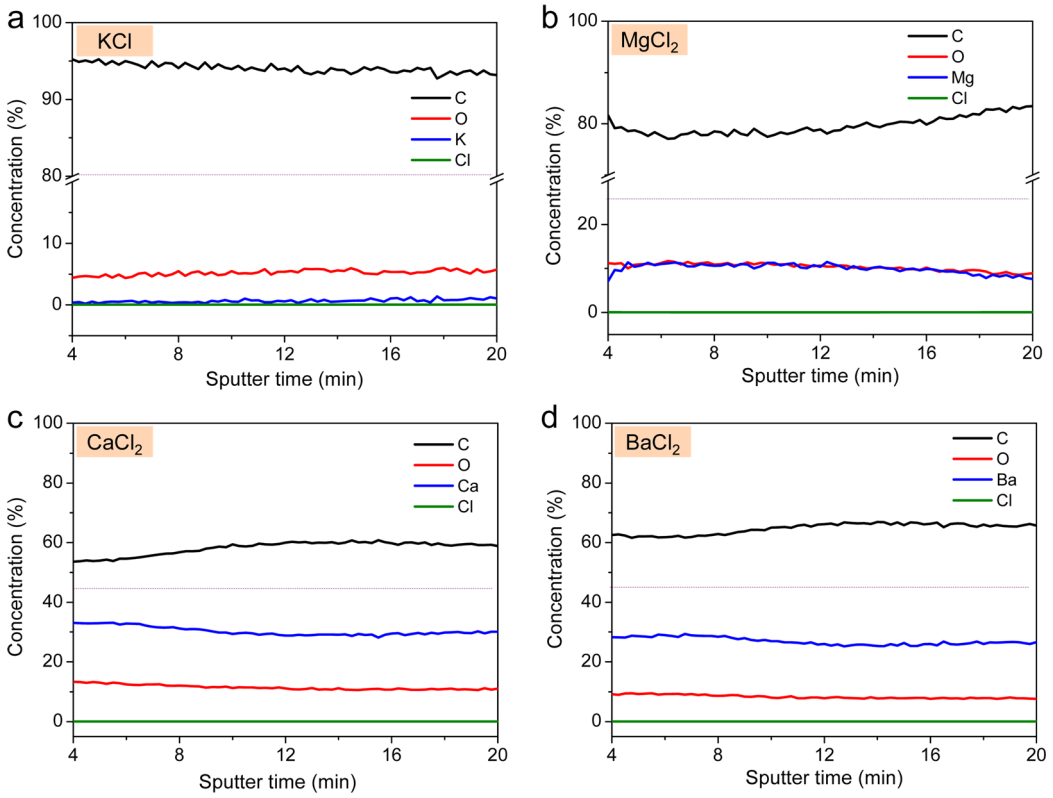

Figure 4. AES spectra for G−O membranes after the penetrations of (a) KCl, (b) $MgCl_2$, (c) $CaCl_2$, and (d) $BaCl_2$ solutions. The sputter rate is 13 nm/min for SiO_2.

thickness, while the concentrations of C and O distribute symmetrically, as shown in Figure 4a, suggesting that K^+ experiences a strong interaction when penetrating through G−O membrane. In contrast, as shown in Figures 4b-d, the concentrations of C and alkaline earth cations (Mg^{2+}, Ca^{2+}, and Ba^{2+}) distribute symmetrically with depth, indicating that the alkaline earth cations intercalate into the lamellar G−O membranes to form cation layers in between the G−O sheets. Particularly, in the case of alkaline earth cations, the residual concentration of Mg^{2+} within G−O membrane is smaller while the concentration of Ca^{2+} is slightly higher than that of Ba^{2+} ions, suggesting that the strengths of interactions between cations and G−O sheets are in the order of $Ca^{2+} > Ba^{2+} > Mg^{2+}$. The AES results suggest that the different strengths of interactions between the cations and G−O sheets may be responsible for the different ion transports through G−O membranes.

Alterations of G−O Primary Structure. To further investigate the interactions between the cations and G−O membranes, the chemical structures of G−O membranes after the penetration of alkali and alkaline earth cations were studied by X-ray photoelectron spectroscopy (XPS) (Figure S5, Supporting Information). The spectra reveal that after the penetration of alkali cations, a new peak located below 284 eV appears in the XPS spectra of G−O membranes, indicating the presence of C-cation interactions. However, this peak is absent in the XPS spectra of G−O membranes after the transport of alkaline earth cations. These results further indicate that a strong C-cation interaction exists during the trans-membrane transport of alkali cations through G−O membranes which is stronger than that in the case of alkaline earth cations.

Calculation of the Binding Energies between Metal Atoms and Graphene. To quantify the interaction between metal atoms and graphene, we performed first-principles calculations based on the plane-wave-basis-set density functional theory (DFT) approach. Spin-polarization was included in the calculations. Generalized gradient approximation (GGA) in Perdew−Burke−Ernzerhof (PBE)[11] parameter settings was used for the exchange−correlation functional, and projector augmented wave (PAW)[12] potentials were used for ion-electron interaction. We used the Vienna Ab-inito Simulation Package (VASP) for the calculations.[13] For all results presented, an energy cutoff of 550 eV was used for the plane-wave basis sets. A supercell with size $1.236 \times 1.282 \times 0.74$ nm^3 was constructed to describe the interlayer gallery between graphene layers. The interlayer distance is 0.74 nm, close to the reported value for graphene oxide (Figure 5a). A 3 × 3x6Monkhorst-Pack k-point grid was used for the Brillouin zone integration. These settings were verified to achieve a total energy convergence less than 1 meV per atom. For geometry relaxation, the force on atoms converged below 0.01 eV/Å. All structures were optimized using the conjugated gradient method. It should also be noted

that the high computational demand prevents DFT calculations to include explicit solvent, and thus the effects of chemical environment (e.g., pH, ionic strength, salt, etc.) could not be directly addressed. Optimizing the models in first-principles calculations could eventually solve this issue by minimizing computational demands while keeping the essential chemistry. This is the subject of our ongoing investigation.

The calculation results are presented in Figure 5b, showing the binding energy defined by $E_{GM} - E_G - E_M$, where E_{GM}, E_G and E_M are energies of the graphene–metal hybrid, the isolated graphene and metal atom respectively. The results show clearly that K binds most strongly inside the gallery, followed by Ba, Na, Ca, Cu, and Cd. This binding energy includes both contributions from the binding between metal atoms and graphene layer, as well as the nanosized constriction with $d = 0.74$ nm.

Mechanism Discussion. On the basis of the above experimental and calculation results, the mechanism for the trans-membrane transport of alkali and alkaline earth cations through G–O membranes is discussed based on the well-known cation–π interactions in biological systems. G–O can be viewed as graphene flakes decorated by several types of oxygen-containing functional groups (e.g., hydroxyl, epoxy and carboxyl groups) on the basal plane and the sheet edge.[7] These functional groups tend to cluster, resulting in ordered sp^2 regions isolated within the sp^3 oxidized matrix. This unique structure facilitates the coordination of transition metal ions with the sp^3 C–O matrix and the cation–π interactions between cations and sp^2 clusters, which will result in the ion-recognition of G–O sheets. After stacking the G–O flakes together to form lamellar membranes (Scheme 1 and Figure 1), the unoxidized area in each sheet will connect each other across all the stacking layers to form a network of nanocapillaries. The formation of hexagonal ice bilayer within the nanocapillaries and the melting transition of ice at the edges of the G–O sheets are responsible for the anomalous water permeation through G–O membranes.[2] However, in the presence of ions within the G–O membranes, due to the interactions of different ions with water molecules, the structure of ice bilayer might be distorted to various extents, which will result in a higher barrier for aqueous solution to penetrate through G–O membranes compared to water (as illustrated in Scheme 1).

Notably, in the case of $NaHSO_4$, the presence of H^+ within the G–O membranes will not cause significant distortion on the structure of ice bilayer due to its tiny size and the collective migration of water within the ice bilayer will not be disturbed seriously. The small proton will be attracted by the oxygen-containing functional groups and propagate through the hydrogen-bonding networks along the water layers rapidly,[14] which will result in a much faster penetration of H^+ than other ions. Therefore, $NaHSO_4$ exhibits the maximum trans-membrane transport rate (as shown in Figure 2 and Figure S2, Supporting Information).

In terms of the penetrations of counter Cl^- and SO_4^{2-} ions, due to the negatively charged nature of G–O membranes in aqueous solution, the counter Cl^- and SO_4^{2-} anions will confront strong repulsions (demonstrated by the AES results in Figure 4) and the transport of Cl^- and SO_4^{2-} ions will be determined by the electrostatic attractions from the corresponding cations.

In the case of alkali and alkaline earth cations investigated, due to the lack of *d* electrons, they are not able to form coordinate complexes with the G–O sheets like the transition metal ions and only the cation–π interactions between the considered cations and the sp^2 clusters occur within the G–O membranes. The balance between cation–π interaction and the desolvation of the ions is responsible for the selective trans-membrane transport of alkali and alkaline earth cations through G–O membranes. According to our simulation results shown in Figure 5, the binding energies between metal atoms and graphene follow the order of K > Ba > Na > Ca > Cu > Cd, which reveals that the cation–π interactions of main group metal ions with graphene are stronger than those of transition metal cations, further demonstrating our speculation that transition metal cations will preferentially coordinate to the sp^3 matrix while cations lacking *d* electrons will bind to the sp^2 clusters of G–O membranes through cation–π interactions. However, in aqueous environment, the water molecules that directly coordinate the cations neutralize the charge of the cations and suppress the interactions of cations with the π clusters,[15] leading to the reordering of the strengths of the cation–π interactions. Notably, due to the higher solvation energy of alkaline earth cations, the screening effect of the hydration shell is stronger than that of alkali cations and the decrease in alkali cation–π interaction energy is much lower than alkaline earth cation complexes (e.g., the solvated K^+–π interaction energy is about three to four times lower, while the solvated Mg^{2+}–π interaction energy is 14 times lower than the bare cation–π interaction energies).[15] Therefore, the penetrations of hydrated alkali cations are relatively smaller than the cognation alkaline earth cations (as shown in Figure 2a).

In the case of hydrated alkali cations (Na^+ and K^+), the cation–π binding of K^+ ion is preferred over Na^+ ion, which is attributed to the higher hydration energy of the smaller Na^+ ions.[16] The interactions between K^+ and π clusters are sufficiently strong to result in partial dehydration of the K^+ ions and the π systems will displace some water molecules from direct contact with the ions, while the Na^+ ions within the nanocapillaries prefer to retain their first hydration shell intact and the π clusters cannot displace waters from the first

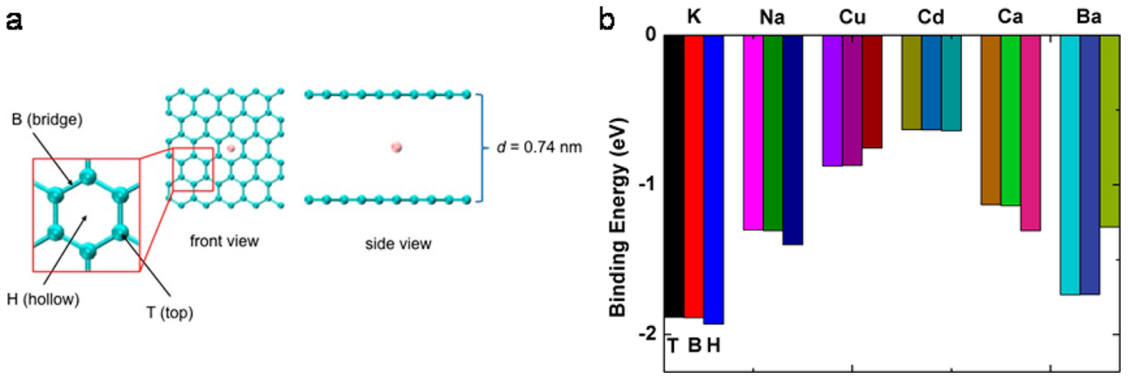

Figure 5. (a) Illustration of the simulation box consisting of an isolated metal atom between graphene layers. The metal atom is placed on top of different positions in the graphene sheet (H: hollow, T: top, B: bridge). (b) Calculated binding energies of metal atoms (K, Na, Cu, Cd, Ca, Ba) in the interlayer gallery between graphene layers.

solvation shell of Na^+.[17] These results indicate that the transport rate of K^+ is much smaller than that of Na^+ due to its strong affinity with the sp^2 clusters within the G–O membranes (in accordance with the results in Figure 2a and Figure 5b).

As for alkaline earth cations (Mg^{2+}, Ca^{2+}, and Ba^{2+}), the electrostatic interactions of cations with the surrounding water molecules and the cation–π interactions between the metal ions and sp^2 clusters are expected to play a major role in the solvent-exchange reactions of hydrated cation with π systems.[18] In the case of Mg^{2+}, due to the much smaller size of Mg^{2+} than Ca^{2+} and Ba^{2+} (Table S1, Supporting Information), the hydration energy is much larger for Mg^{2+} ions. Therefore, sufficient amount of water molecules are attached to the Mg^{2+} ions within the G–O nanocapillaries, which provide adequate shielding that prevents the sp^2 clusters from closely interacting with the Mg^{2+} ions. In contrast, due to the larger sizes of Ca^{2+} and Ba^{2+}, individual water molecules are much more weakly bound. They cannot attract enough water molecules to provide an effective screening, which results in a significant cation–π interaction between the metal ions (Ca^{2+} and Ba^{2+}) and the π clusters. On the basis of the above information, the interactions of hydrated Ca^{2+} and Ba^{2+} ions with the sp^2 clusters are stronger than that of hydrated Mg^{2+} within the G–O nanocapillaries, resulting in a much faster transport rate of Mg^{2+} through G–O membranes compared to Ca^{2+} and Ba^{2+} (as shown in Figure 2a and Figure S2 (Supporting Information) and supported by the AES results in Figures 4b–d).

In terms of the thermodynamics of the trans-membrane transport of alkali and alkaline earth cations through G–O membranes, when the temperature is increased from 10 to 20 °C, the penetrations of K^+, Ca^{2+}, and Ba^{2+} are not changed significantly, while the penetration of Mg^{2+} increases markedly (Figure 4). This is due to the much smaller size and mass of Mg^{2+} compared to K^+, Ca^{2+}, and Ba^{2+} (Table S1, Supporting Information) which allow sufficient stimulation of the thermal motions of Mg^{2+} to compete with the cation–π interactions with the sp^2 clusters within the G–O nanocapillaries at a very small temperature increment. In the case of Mg^{2+}, the thermal motion plays a dominate role when the temperature is increased to 20 °C, while in the case of K^+, Ca^{2+}, and Ba^{2+}, due to their larger masses and sizes, inadequate thermal motions are generated and the cation–π interactions still dominate the penetrations through G–O membranes. When the temperature is increased further, the penetrations of K^+, Ca^{2+}, and Ba^{2+} exhibit a significant enhancement while the penetration of Mg^{2+} do not change markedly (Figure 4), indicating that the thermal motions of K^+, Ca^{2+} and Ba^{2+} begin to play a dominant role with the further increase of temperature. Notably, the penetration increment of K^+ is much greater than those of Mg^{2+}, Ca^{2+} and Ba^{2+} when the temperature is increased from 10 to 40 °C, which might be attributed to the much more serious weakening of the cation–π interaction by the thermal disturbance for K^+ than for Mg^{2+}, Ca^{2+}, and Ba^{2+}. In the case of alkaline earth cations (Figure 3b–d), as the temperature is increased from 10 to 40 °C, the enhancement of thermal motion decreases in the order of $Mg^{2+} > Ca^{2+} > Ba^{2+}$ due to the gradual increase of masses and sizes (Table S1, Supporting Information). The generated thermal motion with the increase of temperature becomes gradually less competitive than the cation–π interactions and the penetration increment with temperature displays a size- and mass-dependent behavior with the order of $Mg^{2+} > Ca^{2+} > Ba^{2+}$, as shown in Figure 3b–d.

CONCLUSION

In summary, we have investigated the selective trans-membrane transport properties of alkali and alkaline earth cations through a membrane composed of stacked and overlapped nanosize and microsize G–O sheets. The thermodynamics of the ion-transport process through G–O membranes is studied and the interactions of the considered metal atoms with graphene are quantified by first-principles calculations based on the plane-wave-basis-set density functional

theory (DFT) approach. These results suggest that the competition between the cation−π interactions of alkali and alkaline earth cations with the sp^2 clusters within the G−O nanocapillaries and dehydration effect of ions is responsible for the ion recognition of G−O membranes, which is similar to some ion transport processes across cellular membranes involving the interactions between cations and aromatic side chains of the hydrophobic amino acids.[8] These experimental and simulation results are consistent with the concept of cation−π interactions involved in biological systems and can help us better understand the ion-transport process through G−O membranes, from which the possibility of modeling the ion-transport behavior of cellular membranes using G−O can be discussed further. Moreover, the ion-recognition property makes G−O membrane a promising candidate in membrane separations.

MATERIALS AND METHODS

G−O Preparation. G−O was synthesized by the modified Hummers' method using potassium permanganate, sulfuric acid, and sodium nitrate. Nanosize G−O sheets with a lateral size of several hundred nanometers were prepared using wormlike graphite as the source[19,20] and microsize sheets were prepared by the same method with natural graphite sources directly.[21,22] The G−O was used to form G−O membranes according to prior method.[3]

Penetration Test. The ion-penetration experiments were conducted with a homemade permeability apparatus. Briefly, a plastic sink (source) separated by a plastic plate from the drain sink with an aperture (~5 mm in diameter) in the center was utilized. The aperture was sealed with G−O membrane by a piece of two-sided copper tape with the same sized hole in the center so that the G−O membrane directly contacted the solutions in source and drain (Figure S1, Supporting Information). Certain aqueous solution (100 mL, 0.1 mol/L) and deionized water were injected into the two separated sinks with the same speed, and the conductivity variations of the filtrates were measured and plotted, which can be used to reflect the permeability of the cations investigated. During the conductivity measurements, the solutions in drains were stirred thoroughly in order to eliminate the concentration differences in bulk solutions and the electrode was fixed at the same place in drains. In order to study the thermodynamic behavior of the ion trans-membrane transport process, control experiments of permeation for K^+, Mg^{2+}, Ca^{2+}, and Ba^{2+} were conducted with G−O membranes composed of nanosize sheets at 10, 20, 30, and 40 °C, respectively.

Characterizations. As-prepared G−O membranes were characterized by optical microscope (ZEISS, Axio Scope.A1), scanning electron microscope (SEM, LEO 1530, 10 kV), atomic force microscopy (AFM, Agilent 5100), and X-ray diffraction (XRD, Siemens, 08DISCOVER, λ=0.15405 nm). During the penetration experiments, the conductivities of the filtrates were measured by a conductivity meter (INESA, DDS-307). After penetration, the G−O membranes were characterized using Auger electron spectroscopy (AES, PHI 700, sputter rate: 13 nm/min for SiO_2) and X-ray photoelectron spectroscopy (XPS, PHI Quantera SXM, AlKα).

Conflict of Interest: The authors declare no competing financial interest.

Acknowledgment. This work is supported by Beijing Natural Science Foundation (2122027), National Science Foundation of China (51372133), National Program on Key Basic Research Project (2011CB013000), and Tsinghua University Initiative Scientific Research Program (2012Z02102). The financial support provided to R.B.L. by the National Science Foundation/EPSCoR and by the State of South Carolina is acknowledged. We thank Prof. Nai-Chang Yeh for helpful discussions.

Supporting Information Available: Supplementary data including a photograph of the permeability apparatus, conductivities of the filtrates of studied cations, temperature-dependent penetrations, Arrhenius curves, XPS spectra of G−O membranes, and radius of naked and hydrated ions. This material is available free of charge via the Internet at http://pubs.acs.org.

REFERENCES AND NOTES

1. Nair, N. N.; Wu, H. A.; Jayaram, P. N.; Grigorieva, I. V.; Geim, A. K. Unimpeded Permeation of Water Through Helium-Leak-Tight Graphene-Based Membranes. *Science* **2012**, *335*, 442–444.
2. Boukhvalov, D. W.; Katsnelson, M. I.; Son, Y. W. Origin of Anomalous Water Permeation through Graphene Oxide Membrane. *Nano Lett.* **2013**, *13*, 3930–3935.
3. Sun, P.; Zhu, M.; Wang, K.; Zhong, M.; Wei, J.; Wu, D.; Xu, Z.; Zhu, H. Selective Ion Penetration of Graphene Oxide Membranes. *ACS Nano* **2013**, *7*, 428–437.
4. Koenig, S. P.; Wang, L.; Pellegrino, J.; Bunch, J. S. Selective Molecular Sieving through Porous Graphene. *Nat. Nanotechnol.* **2012**, *7*, 728–732.
5. Cohen-Tanugi, D.; Grossman, J. C. Water Desalination across Nanoporous Graphene. *Nano Lett.* **2012**, *12*, 3602–3608.
6. Garaj, S.; Liu, S.; Golovchenko, J. A.; Branton, D. Molecule-Hugging Graphene Nanopores. *Proc. Natl. Acad. Sci. U.S.A.* **2013**, *110*, 12192.
7. Loh, K. P.; Bao, Q.; Eda, G.; Chhowalla, M. Graphene Oxide as a Chemically Tunable Platform for Optical Applications. *Nat. Chem.* **2010**, *2*, 1015–1024.
8. Dougherty, D. A. Cation−π Interactions in Chemistry and Biology: A New View of Benzene, Phe, Tyr, and Trp. *Science* **1996**, *271*, 163–168.
9. Mahadevi, A. S.; Sastry, G. N. Cation−π Interaction: Its Role and Relevance in Chemistry, Biology, and Material Science. *Chem. Rev.* **2013**, *113*, 2100–2138.
10. Ma, J. C.; Dougherty, D. A. The Cation−π Interaction. *Chem. Rev.* **1997**, *97*, 1303–1324.
11. Perdew, J. P.; Burke, K.; Ernzerhof, M. Generalized Gradient Approximation Made Simple. *Phys. Rev. Lett.* **1996**, *77*, 3865–3868.
12. Blöchl, P. E. Projector Augmented-Wave Method. *Phys. Rev. B* **1994**, *50*, 17953–17979.
13. Kresse, G.; Furthmüller, J. Efficient Iterative Schemes for *ab Initio* Total-Energy Calculations Using a Plane-Wave Basis Set. *Phys. Rev. B* **1996**, *54*, 11169–11186.
14. Karim, M. R.; Hatakeyama, K.; Matsui, T.; Takehira, H.; Taniguchi, T.; Koinuma, M.; Matsumoto, Y.; Akutagawa, T.; Nakamura, T.; Noro, S.; et al. Graphene Oxide Nanosheet with High Proton Conductivity. *J. Am. Chem. Soc.* **2013**, *135*, 8097–8100.
15. Rao, J. S.; Zipse, H.; Sastry, G. N. Explicit Solvent Effect on Cation−π Interactions: A First Principle Investigation *J. Phys. Chem. B* **2009**, *113*, 7225–7236.
16. Kumpf, R. A.; Dougherty, D. A. A Mechanism for Ion Selectivity in Potassium Channels: Computational Studies of Cation−π Interactions. *Science* **1993**, *261*, 1708–1710.
17. Cabarcos, O. M.; Weinheimer, C. J.; Lisy, J. M. Size Selectivity by Cation−π Interactions: Solvation of K^+ and Na^+ by Benzene and Water. *J. Chem. Phys.* **1999**, *110*, 8429–8435.
18. Rodriguez-Cruz, S. E.; Williams, E. R. Gas-Phase Reactions of Hydrated Alkaline Earth Metal Ions, $M^{2+}(H_2O)_n$ (M = Mg, Ca, Sr, Ba and n = 4−7), with Benzene. *J. Am. Soc. Mass Spectrom.* **2001**, *12*, 250–257.
19. Gu, W.; Zhang, W.; Li, X.; Zhu, H.; Wei, J.; Li, Z.; Shu, Q.; Wang, C.; Wang, K.; Shen, W.; et al. Graphene Sheets from Worm-like Exfoliated Graphite. *J. Mater. Chem.* **2009**, *19*, 3367–3369.

20. Sun, P.; Zhu, M.; Ma, R.; Wang, K.; Wei, J.; Wu, D.; Sasaki, T.; Zhu, H. Graphene Oxide/Titania Hybrid Films with Dual-UV-Responsive Surfaces of Tunable Wettability. *RSC Adv.* **2012**, *2*, 10829–10835.
21. Stankovich, S.; Dikin, D. A.; Piner, R. D.; Kohlhaas, K. A.; Kleinhammes, A.; Jia, Y.; Wu, Y.; Nguyen, S. T.; Ruoff, R. S. Synthesis of Graphene-Based Nanosheets *via* Chemical Reduction of Exfoliated Graphite Oxide. *Carbon* **2007**, *45*, 1558–1565.
22. Eda, G.; Fanchini, G.; Chhowalla, M. Large-Area Ultrathin Films of Reduced Graphene Oxide as a Transparent and Flexible Electronic Material. *Nat. Nanotechnol.* **2008**, *3*, 270–274.